Probing Subtle Coordination Changes in the Iron−Quinone Complex of Photosystem II during Charge Separation, by the Use of NO†

Charilaos Goussias,‡,§ Yiannis Deligiannakis,|| Yiannis Sanakis,⊥ Nikolaos Ioannidis,‡ and Vasili Petrouleas*,‡

Institute of Materials Science, NCSR "Demokritos", 15310 Aghia Paraskevi Attikis, Athens, Greece, Laboratory of Physical Chemistry, Department of Environment & Natural Resources, Management, University of Ioannina, Agrinio, Greece, and Department of Biological Applications and Technologies, University of Ioannina, Greece

Received May 31, 2002; Revised Manuscript Received October 21, 2002

ABSTRACT: The terminal electron acceptor of Photosystem II, PSII, is a linear complex consisting of a primary quinone, a non-heme iron(II), and a secondary quinone, $Q_AFe^{2+}Q_B$. The complex is a sensitive site of PSII, where electron transfer is modulated by environmental factors and notably by bicarbonate. Earlier studies showed that NO and other small molecules (CN^-, F^-, carboxylate anions) bind reversibly on the non-heme iron in competition with bicarbonate. In the present study, we report on an unusual new mode of transient binding of NO, which is favored in the light-reduced state ($Q_A^-Fe^{2+}Q_B$) of the complex. The related observations are summarized as follows: (i) Incubation with NO at −30 °C, following light-induced charge separation, results in the evolution of a new EPR signal at $g = 2.016$. The signal correlates with the reduced state $Q_A^-Fe^{2+}$ of the iron−quinone complex. (ii) Cyanide, at low concentrations, converts the signal to a more rhombic form with g values at 2.027 (peak) and 1.976 (valley), while at high concentrations it inhibits formation of the signals. (iii) Electron spin−echo envelope modulation (ESEEM) experiments show the existence of two protein ^{14}N nuclei coupled to electron spin. These two nitrogens have been detected consistently in the environment of the semiquinone Q_A^- in a number of PSII preparations. (iv) NO does not directly contribute to the signals, as indicated by the absence of a detectable isotopic effect (^{15}NO vs ^{14}NO) in cw EPR. (v) A third signal with g values (2.05, 2.03, 2.01) identical to those of an $Fe(NO)_2$(imidazole) synthetic complex develops slowly in the dark, or faster following illumination. (vi) In comparison with the untreated $Q_A^-Fe^{2+}$ complex, the present signals not only are confined to a narrow spectral region but also saturate at low microwave power. At 11 K the $g = 2.016$ signal saturates with a $P_{1/2}$ of 110 μW and the $g = 2.027/1.976$ signal with a $P_{1/2}$ of 10 μW. (vii) The spectral shape and spin concentration of these signals is successfully reproduced, assuming a weak magnetic interaction (J values in the range 0.025−0.05 cm^{-1}) between an iron−NO complex with total spin of $^1/_2$ and the spin, $^1/_2$, of the semiquinone, Q_A^-. The different modes of binding of NO to the non-heme iron are examined in the context of a molecular model. An important aspect of the model is a trans influence of Q_A reduction on the bicarbonate ligation to the iron, transmitted via H-bonding of Q_A with an imidazole ligand to the iron.

An iron−quinone complex acts as the terminal electron acceptor of PSII[1]. The complex consists of two plastoquinone molecules, Q_A and Q_B, separated by a non-heme iron(II) ion. This general arrangement, which is derived mainly from spectroscopic studies and protein-sequence comparisons (for reviews see refs *1* and *2*) is also supported by the recent crystal-structure determination (*3*), but the data are yet too coarse to provide significant new information, except to indicate an iron to the center of the Q_A ring distance of 10.5 Å. The two quinones operate as sequential electron acceptors, Q_A being a one- and Q_B a two-electron acceptor. Electron transfer rates between the two quinones are in the range of a few tenths of a millisecond, but these vary depending on the treatment. Treatments that change the coordination environment of the iron exert usually a strong influence on the electron-transfer rates. The Fe(II) is coordinated by four histidines, two from each of the two protein subunits D1 and D2. Compared to the photosynthetic bacteria, there are

† This work was supported by TMR Network Grant ERBF-BICT983497 and the Greek Secretariat of Research and Technology (PENNED 99ED75).

* To whom correspondence should be addressed. Tel: +3010 6503312. Fax: +3010 6519430. E-mail: vpetr@ims.demokritos.gr.

‡ NCSR "Demokritos".

§ Present address: Service de Bioénérgetique, URA 2096 CNRS, CEA Saclay, 91191 Gif-sur-Yvette, France.

|| Laboratory of Physical Chemistry, University of Ioannina.

⊥ Department of Biological Applications and Technologies, University of Ioannina.

[1] Abbreviations: PSII, photosystem II; EPR, electron paramagnetic resonance; ESEEM, electron spin−echo envelope modulation; Q_A and Q_B, the primary and secondary quinone electron acceptors of PSII; Ferroquinone complex or $Q_AFe^{2+}Q_B$, the complex of the two quinones and the non-heme iron that is located between them; Pheo, pheophytin; Y_D, redox-active tyrosine on the D2 polypeptide of PSII; Y_Z, redox-active tyrosine on the D1 polypeptide of PSII; S_1 and S_2, the dark stable and the one-electron oxidized state of the electron-donor side of PSII; atrazine, 6-chloro-*N*-ethyl-*N*′-(1-methylethyl)-1,3,5-triazin-2,4-diamine; DCMU, 3-(3,4-dichloro-phenyl)-1,1-dimethylurea; MES, morpholine−ethane−sulfonic acid.

10.1021/bi026223e CCC: $22.00
Published on Web 11/20/2002

important differences in the fifth and sixth coordination positions. In bacteria, these are occupied by a glutamate residue, which acts as a bidentate ligand (*4*). In PSII, at least one of these positions is occupied by bicarbonate (*5*). According to FTIR studies, bicarbonate binds as a bidentate ligand in the reduced state of the non-heme iron and monodentate in the oxidized state (*6*). In PSII, unlike the photosynthetic bacterial counterpart where no ligand displacement has been reported, a number of molecules can bind at the non-heme iron in apparent competition with bicarbonate, resulting, in most cases, in a reversible deceleration of the electron transfer. A direct demonstration of exogenous ligand binding at the iron site has been provided by treatment with nitric oxide. This gives rise to a pronounced EPR signal at $g = 4.0$, characteristic of an iron−nitrosyl complex with $S = {}^3/_2$ (*7*).

Apart from NO (*5*, *7*), a number of anions, mainly carboxylates but also cyanide, bind at the non-heme iron in apparent competition with NO or bicarbonate (*8*). Of particular interest are the effects of cyanide, which appears to bind stepwise (*9*). Cyanide, with an approximate K_d of 10−20 μM, eliminates the $g = 4.0$ signal induced by NO. At higher concentrations, $K_d = 0.1-0.2$ mM, CN^- causes a shift of the $Q_A^-Fe^{2+}$ signal to $g = 1.98$, and with an approximate K_d of 1.2 mM, it converts the iron to low spin ($S = 0$) (*10*). The cyanide experiments imply that up to three sites at (or near) the non-heme iron are accessible to exogenous ligands. The data do not provide direct evidence that all cyanides bind as iron ligands. It is expected, however, that conversion of the iron ion to its low-spin form would require the binding of more than one CN^- ligand. Recently, direct evidence has been provided for the simultaneous binding of F^- and NO on the iron (*11*).

In the reduced state, Q_A^-, the primary quinone ($S = {}^1/_2$) interacts magnetically with the non-heme iron ($S = 2$). This results in a severe broadening of the EPR spectrum of the semiquinone and the appearance of features in the $g = 1.6-1.9$ region (*12*−*14*). Changes in the coordination of the iron modify these signals. Notable is the effect of formate which causes an enhancement of a particular form of the $Q_A^-Fe^{2+}$ signal at $g = 1.82$ (*15*). Cyanide, on the other hand, at moderate concentrations shifts the signals to $g = 1.98$ (9), while at even higher concentrations, it converts the iron to $S = 0$, revealing the unperturbed free semiquinone signal at $g = 2.045$ (*10*). Unlike the bacterial counterpart, where a thorough theoretical analysis has been carried out (*16*, *17*), little effort has been made to simulate the various $Q_A^-Fe^{2+}$ signals in PSII, despite their variety and their likely association with a physiological control of the electron transfer rate. Recently the $Q_A^-Fe^{2+}$ signal in the presence of NO bound on the iron with or without fluoride present has been analyzed in detail. The system of the two half-integer interacting spins ($^1/_2$ for the semiquinone and $^3/_2$ for the iron−NO complex) with components in perpendicular and parallel mode EPR (at X- and Q-band microwave frequencies) has been successfully simulated with an antiferromagnetic coupling of 0.5 cm^{-1} in the presence, and 1.3 cm^{-1} in the absence of F^- (*11*).

In this study, we present a new set of EPR signals induced by NO, or NO + CN^- binding in the reduced state, $Q_A^-Fe^{2+}$, of the iron−quinone complex. The signals appear close to the $g = 2$ region, but at somewhat higher g values, and unlike all other signals from the complex (with the exception of the free semiquinone signal), they saturate at low microwave powers. On the basis of the phenomenology of the signal production the ESEEM spectra and the theoretical analysis, the signals are assigned to Q_A^-, interacting very weakly with an $S = {}^1/_2$ iron−nitrosyl complex. NO binds at the iron in a new mode, separate from the one producing the $g = 4$ signal. Interestingly enough, affinity for this site is enhanced by the reduction of Q_A. The results are discussed in the context of a molecular model. An important aspect of the model is a trans influence of Q_A reduction on the bicarbonate ligation to the iron, transmitted via H-bonding of Q_A with an imidazole ligand to the iron.

MATERIALS AND METHODS

PSII-enriched thylakoid membranes were isolated from market spinach by procedures described elsewhere (*18*, *19*). Samples for EPR measurements were suspended in 0.4 M sucrose, 15 mM NaCl, and 20 mM MES, pH 6.5, at 3−3.5 mg of chl/mL. Some experiments were carried with Tris-treated PSII samples, prepared as follows. BBY samples (∼1 mgr Chl/mL final concentration) were incubated for 20 min with 0.8 M Tris (pH 8.3) for 20 min under dim light. Excess Tris was subsequently removed by centrifugation and the samples were resuspended to an SMN buffer at pH 6.5 (50 mM MES).

^{14}NO (99.5% pure) was purchased from Messer Griesheim Co. ^{15}NO was synthesized by acidification of a $K^{15}NO_2$ aqueous solution (99% enrichement in ^{15}N, supplied by Isotec Inc.). The NO treatment was carried out anaerobically in EPR tubes at 0 °C, by slowly bubbling 5 mL of a given mixture of NO and N_2, typically 10% to 20% in NO. This results in NO concentrations of 0.2 or 0.4 mM, respectively, which are very reproducible, as measured by the characteristic EPR peak of NO in the $g = 2$ region. The free NO peak often declined during successive treatments (possibly due to NO dimerization or nonspecific reactions) and this resulted in baseline distortions in difference spectra.

Some experiments were performed with pulverized BBY membranes. BBY membranes are painted on Mylar sheets and frozen in liquid nitrogen. Subsequently, the frozen material is scraped from the Mylar and transferred into an EPR tube. The thin flakes are further pulverized at liquid nitrogen temperatures with a thin aluminum rod. The air that liquefies inside the tube, because of the low temperature, is removed by vacuum before the NO insertion. The whole procedure is performed in the dark.

Illumination of the samples was performed in a glass dewar flask with a 340 W projector lamp, filtered through a solution of $CuSO_4$.

Continuous wave EPR spectra were recorded using a Bruker ER-200D-SRC spectrometer interfaced to a personal computer and equipped with an Oxford ESR 9 cryostat, an Anritsu MF76A frequency counter, and a Bruker 035M NMR gaussmeter. Microwave power saturation data were fitted with the formula $\log (I/\sqrt{P}) = C - b/2 \log(1 + P/P_{1/2})$, where I is the intensity of the signal, P the microwave power and $P_{1/2}$ the microwave power for half-saturation, C the concentration of spins, and b an inhomogeneity parameter with a value of 0.95 in the present fittings (*10*).

Pulsed EPR was performed with a *Bruker* ESP 380 spectrometer with a dielectric resonator. In the three-pulse

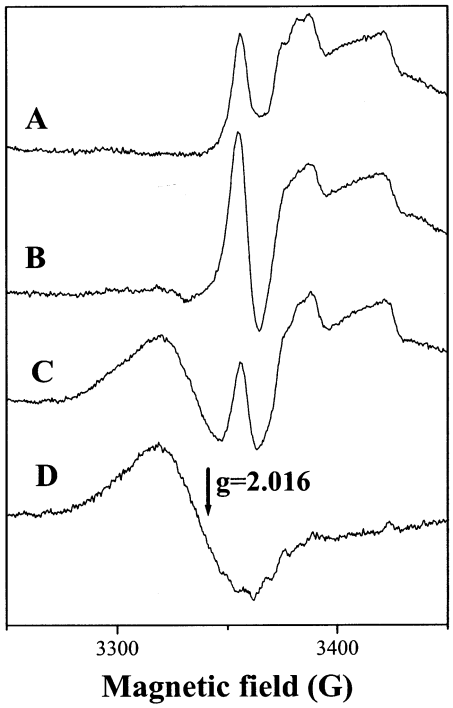

FIGURE 1: Formation of the $g = 2.016$ EPR signal. A sample was (A) treated with 0.4 mM NO for a few minutes, (B) illuminated at 200K, and (C) incubated subsequently in the dark at −30 °C for 30 min. Spectrum D is the difference between spectra C and A. EPR conditions: temperature, 11 K; microwave frequency, 9.41 GHz; modulation amplitude, 4 G_{pp}; microwave power, 50 μW.

($\pi/2-\tau-\pi/2-T-\pi/2$) ESEEM data, the amplitude of the stimulated echo as a function of $\tau + T$ was measured at ~9.7 GHz. The minimum interpulse $\tau + T$ was 48ns and was incremented in steps of 8 ns. The duration of the $\pi/2$ pulse was 16 ns, corresponding to an excitation profile of $H_1 \sim 9$ G. To remove the unwanted echoes in a three-pulse experiment, the phase-cycling procedure described in (*20*) was applied. Before Fourier transformation, the time-domain echo decay was factored out by subtraction of a linear function. The field-swept spectra were obtained by recording the integral of the echo as a function of the magnetic field after a two-pulse sequence ($\pi/2-120ns-\pi$); the duration of the $\pi/2$ and π pulse was 64 and 128 ns, respectively, and the integration gate was 200 ns. Theoretical simulations of the ESEEM spectra where performed by numerical diagonalization of the pertinent spin-Hamiltonian for an $S = {}^1/_2$, $I = 1$ spin system as described in ref *21*.

RESULTS AND DISCUSSION

A New EPR Signal at g = 2.016. Incubation of PSII membranes for less than 5 min at 0 °C with low-to-moderate NO concentrations, 0.3−0.5 mM, results in the rapid interaction of NO with $Y_D^\bullet$ (*5*), the oxidation of cyt b_{559} (Goussias et al., unbublished results), and low levels of the signal at $g \sim 4.0$, due the relatively slow binding of NO to the non-heme Fe^{2+} (*5*). If the sample is subsequently illuminated at 200 K and incubated in the dark at 30 °C for 10−30 min, a new EPR signal develops. The experiment is described in Figure 1.

Figure 1A shows the spectrum of a sample incubated with 0.4 mM NO for a few min. In this spectral region the spectrum contains a broad contribution from free NO at high fields (*5*), as well as a narrow contribution of unknown origin at $g = 2$. No signal II contribution is observed in the spectra due to the rapid interaction of NO with tyr $D^\bullet$, which results in the formation of a diamagnetic species (*5*, *22*). Illumination at 200 K of the sample, Figure 1B, results in no significant changes except for an increase in the $g = 2$ region attributed to a minority radical species (e.g., a chlorophyll species acting as a donor in a minority of the centers). Potential contributions at $g < 2$ from the iron−quinone complex would be too weak to be detected under the present experimental conditions. Subsequent incubation at −30 °C results in the formation of a new signal, Figure 1C. The signal, which is more clearly shown as a difference spectrum (Figures 1C − Figure 1A) in Figure 1D, has the form of a derivative with a zero-crossing point at $g = 2.016$ and will be called hereafter the $g = 2.016$ signal.

Conditions that Affect Production of the Signal. Preincubation at −30 °C in the dark of NO-treated samples does not induce the signal. Following the 200 K illumination, a very low signal level can be discerned in the spectrum of Figure 1B, but the signal develops efficiently at −30 °C with an approximate halftime of 10 min. Direct illumination for a few minutes at −30 °C induces only part of the signal; the size of the signal corresponds to what one would obtain by incubation of a preilluminated sample at −30 °C for the same amount of time. Further incubation in the dark at this temperature leads to a full-size signal. It appears that charge separation initiates a reaction that proceeds in the dark in the tens of min scale at −30 °C. Further evidence is provided in the next section.

Following the illumination, the signal can be also induced by incubation at −20 °C but not at −10 °C or higher temperatures. Incubation at −10 °C or higher temperatures, after the signal induction at −30 °C, results in elimination of the signal in 5 min at −10 °C and less than 1 min at +10 °C (see a later section for the induction of weak new signal under these conditions). Prolongation of the incubation period at −30 °C beyond 30 min (charge recombination or secondary charge transfer occurs following this prolonged incubation) also results in gradual signal disappearance. To form the signal again, a new low-temperature illumination is necessary.

The g = 2.016 is Induced by the Interaction of NO with PSII in the Charge-Separated State and Is Assigned to the Ferroquinone Acceptor. To exclude the possibility that photochemistry of the NO molecule itself triggers the effects observed, the NO-treatment/illumination-at-200 K sequence was reversed in the following experiment. In the presence of both 100 μM atrazine (which inhibits electron transfer from Q_A^- to Q_B) and 80 mM formate (which slows charge recombination between Q_A^- and the donor side), Q_A^-, induced by prior illumination at 200K, is stable for several minutes at 0 °C (*23*). Treatment of such a sample with NO at 0 °C within the lifetime of Q_A^- and subsequent incubation at −30 °C for several minutes induced a sizable signal (Figure S1 of Supporting Information). Actually, the signal could be reversibly lost by warming up to 10 °C for 1 min and recovered by incubation at −30 °C within the lifetime of Q_A^- without additional 200 K illumination. This experiment indicates that Q_A^- is a prerequisite for signal formation. The reversible signal loss at +10 °C appears to indicate a thermally activated disordering of the structure that produces

the signal, or dissociation of NO from its binding site.

Double integration of the $g = 2.016$ signal area indicates an abundance of 40−60% compared to the PSII concentration. The estimation is based on a comparison with the maximum Signal II size from Y_D, obtained after illumination at 0 °C of an untreated sample.

The signal can be induced in Tris-treated PSII membranes, which lack the Mn complex and the three extrinsic polypeptides. In these preparations, the cytochrome is in a low-potential form and is spontaneously oxidized giving an EPR signal at $g = 2.95$. The procedure for induction of the $g = 2.016$ signal does not influence the $g = 2.95$ signal, indicating that the cytochrome b_{559} is not responsible for the 2.016 signal. In intact PSII membranes, the majority of the cytochrome is in its high-potential form and is normally in the reduced state. Upon addition of NO, the cytochrome is immediately oxidized (Goussias Ch. and Petrouleas V., unpublished results) and remains completely oxidized and unchanged during the entire treatment. Correlation of the $g = 2.016$ signal with Y_D is also unlikely. In most of the samples, significant levels of oxidized and reduced tyrosine were present in the dark, but the evolution of the signal requires prior illumination, as stated above. The signal is also completely formed in PSII membranes with Y_D fully reduced (with sodium ascorbate) or fully oxidized (by illumination at 0° C), before the NO treatment. The relatively long times required for the development of the signal also exclude association with the transiently formed radicals P_{680}^+, $Y_Z^\bullet$, Chl^+, or $Pheo^-$. The only long-lived component invariably formed under all the above conditions is the reduced primary quinone electron acceptor, Q_A^-. The signal must therefore be associated with this radical species interacting with the non-heme iron, this interaction being modified by NO.

A note on the lifetime of Q_A^- is required at this point. In the absence of NO, Q_A^- decays via charge recombination, or secondary electron transfer to Q_B in those centers that have Q_B bound. In untreated preparations under normal circumstances, illumination at 200 K advances S_1 to S_2 concomitant to the reduction of Q_A. The S_2 Q_A^- couple recombines with a halftime of a few min at −30 °C. In the presence of NO S_2 is rapidly reduced to S_1 (and more slowly to lower S states) (*24*) explaining the extended lifetimes of Q_A^- observed in the present experiments.

ESEEM Experiments Support the Association of the $g = 2.016$ Signal with Q_A^-. Electron spin−echo envelope modulation (ESEEM) spectroscopy can provide direct evidence regarding the amino acid environment of the $g = 2.016$ spin system, and therefore can offer a critical test of the association with the semiquinone Q_A^- radical.

The echo-detected field-swept spectrum of samples treated with NO, illuminated at 200 K and subsequently incubated at −30 °C so as to develop the $g = 2.016$ signal, is displayed in the inset of Figure 2A (solid line). In this absorption-mode EPR spectrum the $g = 2.016$ signal is manifested as a bump, marked by the arrow. In the corresponding first-derivative spectrum, produced by numerical differentiation (dashed line), the signal becomes evident. The high-field part of the signal is masked by the strong broad signal from free NO.

In Figure 2A the time-domain three-pulse-ESEEM trace recorded at 5 K and a magnetic field of 3427 G is displayed. The nonmodulated part of the signal has been subtracted to facilitate a better visualization of the modulation. We have carefully looked for possible interference from other background EPR signals, which might contribute in the same field region. At a magnetic field shifted by up by 60 G, i.e., 3367 G, essentially no modulation was recorded under the same experimental conditions. Only much shallower modulations, with frequencies at ∼3 and ∼7 MHz, corresponding to those reported earlier for the cyt b_{559} (*25*) were recorded, but these were much weaker than the modulation at 3427 G. Thus, we conclude that ESEEM signals from the cyt b_{559} contribute minimally to the signals at 3427 G discussed in the present paper. No other background ESEEM signals are practically detectable at other field settings. Therefore, under the conditions of our experiments, the ESEEM signal displayed in Figure 2 is exclusively due to the spin system giving rise to the $g = 2.016$ EPR signal.

The stimulated-echo decay was recorded at 20 different τ values in order to avoid missing modulation frequencies due to suppression effects (*20*, *26*). The time-domain ESEEM signal displayed in Figure 2A is characterized by relatively deep low-frequency modulations. According to the first principles of the ESEEM phenomenon, the modulation is an indication that the electron spin is interacting magnetically with nearby nuclei and that this magnetic interaction does not deviate considerably from the nuclear Zeeman interaction (*27*, *28*). The corresponding frequency-domain spectra, obtained after Fourier transforming the time-domain data, are shown in Figure 2B. Several low-frequency components are resolved at 0.50, 0.92−1.10, 1.70, 1.95, and 2.90 MHz as well as broader components with maxima at ∼5.6 and 7 MHz. These low-frequency features originate from naturally abundant nuclei in PSII, either ^{14}N ($I = 1$) or ^1H ($I = {}^1/_2$), interacting weakly with the electron spin system at resonance at $g = 2.016$. A useful observation is that the sum of the 0.92 and 1.95 MHz frequencies is close to the 2.90 MHz frequency. This is a characteristic indication that these peaks arise from ^{14}N ($I = 1$) nuclear modulation in the case where the nitrogen coupling fulfills, within certain margins, the so-called "cancellation condition", i.e., $A_{iso} = 2\nu_I$ (*27*−*29*). On the basis of ESEEM spectroscopy, it has been shown recently that this type of weak nitrogen coupling can occur between protein amino acid ^{14}N nuclei and the semiquinone Q_A^- in PSII (*29*−*31*, *21*). In the following, based on numerical simulations of the experimental ESEEM spectra, we demonstrate that all the observed modulations in Figure 2 arise from ^{14}N-nuclei.

In the case of exact cancellation, i.e., when $A_{iso} = 2\nu_I$, the ESEEM spectrum contains three sharp low-frequency lines, which are primarily determined by the ^{14}N nuclear quadrupole interaction (*27*). The corresponding ESEEM spectra are typically characterized by maxima at frequencies $\nu_+ = 3K(1 + \eta)$, $\nu_- = 3K(1 - \eta)$, $\nu_0 = 2K\eta$, and a double quantum transition line, $\Delta m_I = 2$, occurring at higher frequencies, typically in the range 4−6 MHz. In cases of considerable deviation from the cancellation condition, the spectral features shift and/or broaden (*27*, *32*). However, if the deviation from the exact cancellation is limited, i.e., such that $|A - 2\nu_I| < 4K/3\nu_I$, then the simple spectral features characterizing exact cancellation are retained, thus allowing a first-order estimation of the nuclear quadrupole parameters K and η directly from the spectrum (*29*). Further refinement

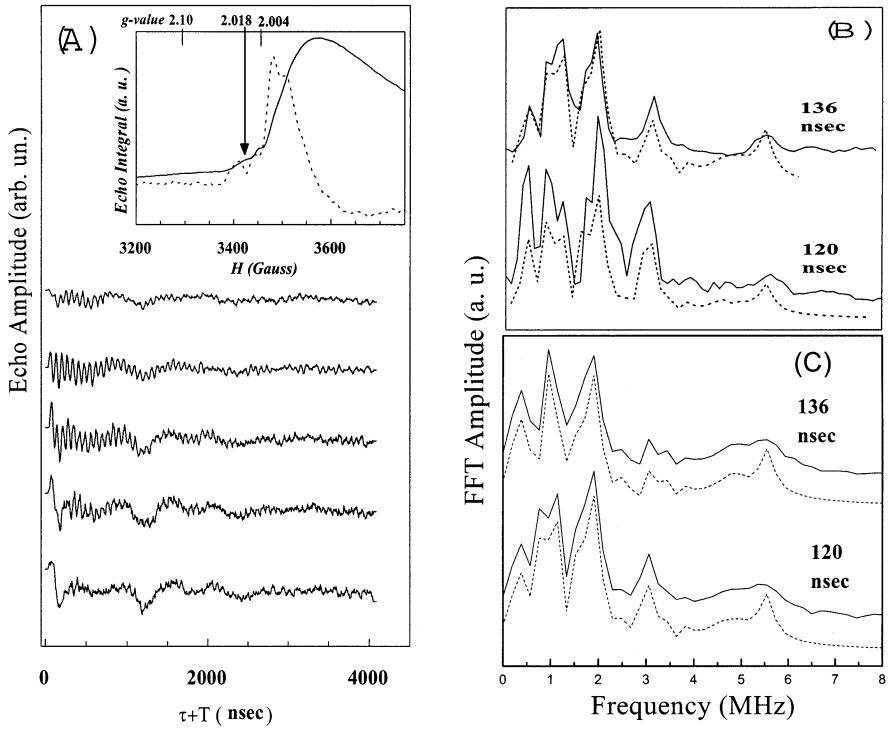

FIGURE 2: (A) Time domain three-pulse ESEEM signals recorded for the $g = 2.016$ signal in PSII. The τ values from top to the bottom are 192, 168, 152, 136, and 120 ns, respectively. Experimental conditions: frequency, 9.69 GHz; magnetic field, 3427 G; temperature 5 K; time interval between successive pulse sets, 6.4 ms; 2000 events were averaged for each time point. For each τ value, the initial T value was 48 ns, and 512 data points were collected at 8 ns intervals; a four-step phase cycle was employed. Inset: (solid line) Integral of the electron spin−echo resulting from a two-pulse sequence, as a function of the magnetic field. Integration gate 200 ns. (dashed line) First derivative of the field-swept echo-detected spectrum, produced by numerical differentiation. The vertical arrow indicates the $g = 2.016$ spectral position. (B) Frequency-domain ESEEM spectra (solid lines) for the $g = 2.016$ signal. The dashed lines represent theoretical spectra obtained by numerical simulations by using two ^{14}N-couling tensors ($\mathbf{N_I}$: $e^2qQ/h = 3.25$ MHz, $\eta = 0.61$, (A_{xx}, A_{yy}, A_{zz}) = (1.3, 2.4, 2.8 MHz). $\mathbf{N_{II}}$: $e^2qQ/h = 1.76$ MHz, $\eta = 0.63$, (A_{xx}, A_{yy}, Azz) = (1.4, 1.4, 2.6 MHz)). (C) Frequency-domain ESEEM spectra (solid lines) for the $g = 2.027/1.976$ signal in the presence of CN^-. The dashed lines represent theoretical spectra obtained by numerical simulations by using two ^{14}N-couling tensors ($\mathbf{N_I}$: $e^2qQ/h = 3.25$ MHz, $\eta = 0.60$, (A_{xx}, A_{yy}, A_{zz}) = (1.5, 2.4, 2.9 MHz). $\mathbf{N_{II}}$: $e^2qQ/h = 1.74$ MHz, $\eta = 0.65$, (A_{xx}, A_{yy}, A_{zz}) = (1.4, 1.4, 2.6 MHz)).

of the quadrupole couplings can be achieved by numerical simulations of the ESEEM spectra. In the present case, the detected lines at 0.92, 1.95, and 2.90 MHz yield $K = 0.81$ MHz and $\eta = 0.61$. The numerical simulation of the ESEEM data verifies the validity of this analysis and allows a more precise estimation of the hyperfine and quadrupole coupling parameters.

The preliminary fitting of the experimental spectra was directed at the simulation of the frequency positions, i.e., the basic line-shapes of the major features in Figure 2B. The Euler angles were then adjusted in order to reproduce the correct relative intensities of the individual lines. Representative simulated ^{14}N spectra are shown in Figure 2B (dashed lines), together with the experimental traces. These spectra have been calculated by using two ^{14}N-tensors. One ^{14}N-tensor, named $\mathbf{N_I}$, is responsible for the prominent features at 0.92, 1.95, and 2.90 MHz. A second ^{14}N tensor, named $\mathbf{N_{II}}$, contributes the features at 0.50, 1.09 and 1.70 MHz in Figure 2B. The two sets of ^{14}N-hyperfine and nuclear quadrupole parameters, used to reproduce the experimental spectrum in Figure 2, are $e^2qQ/h = 3.25$ MHz, asymmetry parameter $\eta = 0.61$, and a hyperfine coupling (A_{xx}, A_{yy}, A_{zz}) = (1.3, 2.4, 2.8 MHz) for $\mathbf{N_I}$. The second ^{14}N coupling, $\mathbf{N_{II}}$, is characterized by $e^2qQ/h = 1.76$ MHz, $\eta = 0.63$, and (A_{xx}, A_{yy}, A_{zz}) = (1.4, 1.4, 2.6 MHz). These two ^{14}N-couplings show strong similarities with the ^{14}N-couplings observed for the semiquinone Q_A^- in PSII (*21*, *30*−*32*). The details of the two ^{14}N-couplings are sensitive to the preparation protocol, i.e., whether the non-heme Fe^{2+} is present (*31*), removed (*30*, *32*), or converted to the low-spin state (*32*), and to a large degree to the pH (*21*). At physiological pH (*6*−*7*) both these ^{14}N− Q_A^- interactions are observed (*30*, *32*) with couplings comparable to those reported here for the $g = 2.016$ signal. (i) In both cases, two protein ^{14}N nuclei are coupled to the electron spin. (ii) In both cases, the two ^{14}N−NQR couplings are similar, indicating that they originate from similar ^{14}N-bearing amino acids. (iii) The size of the ^{14}N-hyperfine couplings observed for the $g = 2.016$ EPR signal is comparable to the size of the ^{14}N-hyperfine couplings detected for the semiquinone Q_A^- in PSII at physiological pH (*21*, *31*, *32*). On the basis of these similarities, we suggest that the $g = 2.016$ EPR signal results from the semiquinone Q_A^- state of PSII. The coupled nitrogens have been assigned to the amide nitrogen of protein backbone and the amino nitrogen of a histidine, respectively, based on a comparison of the e^2qQ/h and η values with ^{14}N-NQR (*33*) and ^{14}N-ESEEM data for PSII (*21*, *30*, *32*). On the basis of the amino acid sequence of the Q_A binding pocket in D2, as discussed previously (*21*, *30*, *32*), the interacting nitrogens are attributed to the NH of Ala 261 and the imidazole of His 215 both from the D2 protein. It should be noted however that the assignment of the second ^{14}N-coupling to His 215 was negatively tested in isotopically labeled *Synechocystis* PSII (*31*). The spin-transfer mechanism

from the Q_A^- onto these nitrogens has been discussed in detail in (*32*).

The ^{14}N hyperfine couplings in the case of the $g = 2.016$ signal, have small, but clear, differences from the previously published $^{14}N-Q_A^-$ interactions (*30*−*32*) in the extent of the rhombicity and the size of the hyperfine couplings. These differences probably originate from changes in the local environment of the Q_A^-, which also perturb the normally strong magnetic coupling between Q_A^- and the non-heme iron, as will be discussed in later sections.

Effects of Exogenous Iron Ligands on the $g = 2.016$ Signal. Comparison with the $g = 4$ ($S = 3/2$) $Fe^{2+}-NO$ Configuration. The above experiments have assigned the $g = 2.016$ signal to the $Q_A^-Fe^{2+}$ state, but the site of binding of NO is not apparent. Given the affinity of the non-heme iron for a number of exogenous ligands, including NO, it is possible that the signal represents a modified form of the $Q_A^-Fe^{2+}$ interaction, due to the binding of NO to the iron. The mode of binding under the present conditions must be different, however, from the binding of NO that produces the EPR signal at $g = 4.0$ (*5*, *11*). The $Q_A^-Fe^{2+}$ state in the latter case gives entirely different EPR signals (*11*). We have examined the effect on the $g = 2.016$ configuration of exogenous molecules that compete or bind simultaneously with NO in the $g = 4.0$ configuration.

Oxalate and glycolate are known to bind at the non-heme iron in competition with the NO-binding that produces the $g = 4.0$ signal (*34*, *35*). Pretreatment with 40 mM sodium oxalate for 1 h at 0 °C in the dark, which is sufficient to fully suppress the $g = 4.0$ signal, resulted in only a small decrease in the size of the $g = 2.016$ signal. Glycolate under similar conditions suppressed the $g = 2.016$ signal by 40% compared with 80% suppression of the $g = 4$ signal (*35*). Formate, which has been studied extensively for its effects on the ferroquinone complex in competition with bicarbonate, enhances by its binding the rhombicity of the $g = 4$ signal (*5*) but induces no changes on the $g = 2.016$ signal. As a matter of fact, formate was present in some of the experiments described in previous paragraphs. These observations imply that the carboxylate anions bind weakly and/or the affinity of NO for the iron is high in the $Q_A^-Fe^{2+}$ state of the ferroquinone complex. Actually, the former possibility was implied by earlier studies of the light induced oxidation of the iron in the presence of a number of carboxylate anions. Unlike the straightforward oxidation of the iron by ferricyanide, which is characterized by diverse changes indicative of the binding of the various anions (*34*), the light-induced oxidation (a procedure that requires reduction of an exogenous quinone via Q_A^- (*36*, *37*) produced similar Fe^{3+} spectra in the absence or presence of a number of the carboxylate anions (Deligiannakis, Y., and Petrouleas, V., unpublished observations). The experiments implied that these anions were displaced during the step (single-electron reduction of the iron quinone complex) that precedes the iron oxidation.

In Figure 3, we compare the size of the $g = 2.016$ signal in the absence and presence of fluoride. In this experiment the incubation with NO (and fluoride) was extended to 1 h. Under these conditions, the majority of the iron has NO bound to form the $g = 4$ ($S = 3/2$) species. The light-induced reduction of Q_A^- at 200 K produces well-established changes in the spectra attributed to the magnetic interaction of the spin of the semiquinone with the spin of the iron−nitrosyl

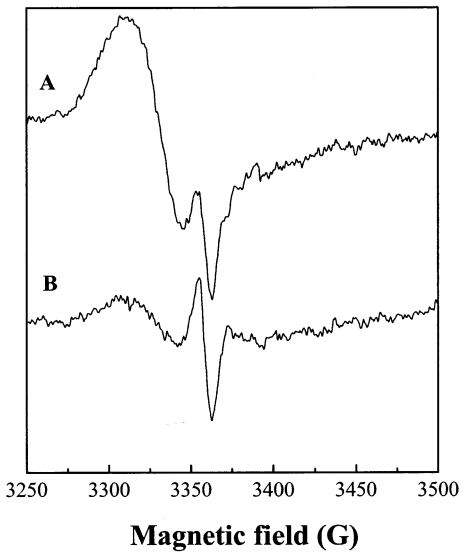

FIGURE 3: Effect of fluoride on the $g = 2.016$ signal. Difference EPR spectra and EPR conditions as in Figure 1. The narrow feature at $g = 2.00$ represents a minority species of unknown origin. The slope of the baseline at high field is due to incomplete subtraction of the free NO contribution. Sample treatment as in Figure 1 except in the presence of (A) 25 mM NaCl or (B) 25mM NaF and extension of the incubation with NO to 1 h.

species (*5*, *11*). The subsequent incubation at −30 °C produces a sizable $g = 2.016$ signal in the control sample (containing 25 mM Cl^-) but a greatly diminished signal in the fluoride containing sample, Figure 3. Assuming that iron is the site of the NO binding that induces the $g = 2.03$ signals (more evidence is provided in subsequent sections), the results indicate a conversion of the "$g = 4$" to the "$g = 2.03$" mode of binding of NO in the control sample but inhibition of this conversion in the presence of fluoride. Qualitatively similar results are obtained following shorter preincubation times with NO or NO and F^-. It should be noted that prolonged incubation times with NO that elicit a strong $g = 4$ signal (absence of fluoride) do not speed up detectably the evolution of the $g = 2.03$ signal.

The effects of cyanide are of particular interest and are examined separately below.

A Modified Signal in the Presence of Cyanide. If the experiment resulting in the formation of the $g = 2.016$ signal is carried out in the presence of modest concentrations of cyanide, a significantly modified signal is obtained. The signal, shown as a difference spectrum in Figure 4, consists of an absorption peak at $g = 2.027$ and a valley at $g = 1.976$. The derivative line at $g \sim 2.00$ does not belong to the signal and may probably arise from a Chl^+ radical. This is inferred from the variable relative intensity of the signals in different samples.

A notable property of the $g = 2.027/1.976$ signal is that, depending on the length of prior incubation with CN^- and NO, it can be induced directly by the illumination at 200 K. In an experiment with two samples treated with 50 mM KCN and subsequently incubated with approximately 0.3 mM NO for 5 or 90 min in the dark, illumination at 200 K induced a small signal in the 5 min sample and a much larger one in the sample incubated for 90 min (Figure S2 of Supporting Information).

CN^- is known to bind at the non-heme iron in a stepwise reaction (*10*): At pH 6.5, CN^- eliminates the $g = 4.0$ signal

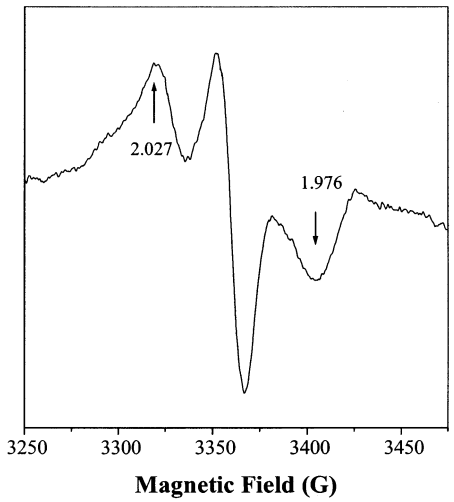

FIGURE 4: The modified signal in the presence of 80mM NaCN (pH 6.5) and 0.2mM NO at 11 K. Difference EPR spectrum obtained as in Figure 1 and with same EPR settings.

resulting from the interaction of ca. 0.3 mM NO with the Fe^{2+} with an apparent K_d of 10−20 μM. At higher concentrations, K_d = 0.1−0.2 mM, CN^- modifies the $Q_A^-Fe^{2+}$ EPR signal to g = 1.98. At even higher concentrations, K_d = 1.2 mM, achieved by raising the pH to 8, cyanide converts the non-heme iron to low spin. The modification of the g = 2.016 signal described in this section is completed at about 80 mM NaCN at pH 6.5 (corresponding to ca. 0.12 mM CN^-), while the signal size decreases at higher CN^- concentrations. Using 200 mM of cyanide resulted in the formation of ca. $^1/_3$ of the signal, compared to the maximum obtained with 80 mM CN^-. Conversion of the non-heme iron to low spin, by 360 mM NaCN at pH 8.1, resulted in no signal formation. These observations suggest that iron is the site of the NO binding that produces the new signals. Furthermore, the observed modification of the signal appears to correlate with the first site/mode of binding of cyanide. Therefore, the binding of one CN^- and perhaps one NO molecule at or in the vicinity of the non-heme iron is responsible for the g = 2.027/1.976 signal formation.

Interconversion of the g = 2.027/1.976 and g = 2.016 Signals. The g = 2.027/1.976 shares similar properties with the g = 2.016 one in that incubation for approximately 1 min at 10 °C eliminates the signal and the presence of formate (80 mM) and atrazine (0.1 mM) does not affect the signal. The extended stability of Q_A^- in the presence of the latter inhibitors allowed the subjection of the 2.027/1.976 signal to −30 °C/+10 °C cycles, as was done with the 2.016 signal in an earlier section. Initial illumination/incubation at −30 °C yielded the g = 2.027/1.976 signal, which disappeared at +10 °C. Subsequent incubation at −30 °C resulted, surprisingly, in the appearance of the g = 2.016 form (Figure S3 of Supporting Information). This suggests that the g = 2.016 signal represents a more stable configuration. Presumably CN^- binds with high affinity in the non reduced state of the iron−quinone complex. Subsequent reduction of Q_A^- by illumination at 200 K favors the binding of the electrophilic NO. The reduced complex with CN and NO simultaneously bound (2.027/1.976 signal) represents probably a metastable configuration, which given the thermal activation energy at 10 °C converts to the NO-alone g = 2.016 configuration. The latter, too, is thermally unstable at 10 °C, but it represents the equilibrium configuration at −30 °C.

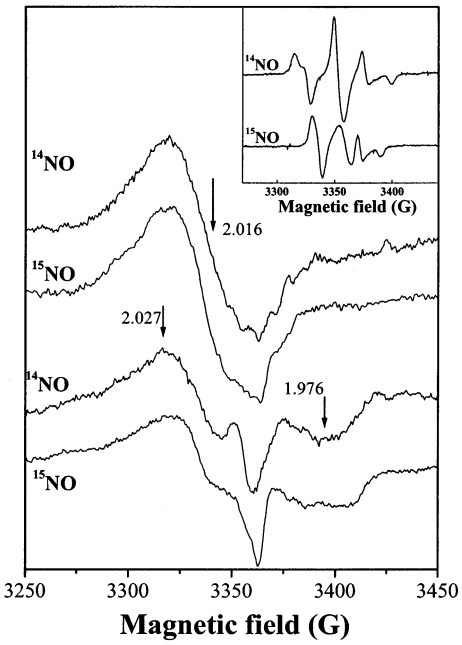

FIGURE 5: Effects of isotopic replacement (^{15}NO instead of ^{14}NO) on the signals. Preparation of the 2.016 and 2.027/1976, respectively, is the same as that in Figures 1D and 4. The inset shows, as a reference, the effect of the isotopic replacement on the tyrosine D iminoxyl radical EPR signal (*22*). EPR conditions are the same as those in Figure 1.

ESEEM Experiments of the 2.027/1.976 Signal. ESEEM experiments indicated that the main features seen in the case of the 2.016 signal, Figure 2B, were also observed for the g = 2.027 signal, Figure 2C. It seems, therefore, that the g = 2.016 (NO alone) and the g = 2.027 and 1.976 (NO + CN^-) originate from the same species, Q_A^-.

Isotopic Replacement, ^{15}NO vs ^{14}NO, Indicates No Detectable Contribution of NO to the 2.016, 2.027/1.976 Signals. Experiments with isotopically labeled NO (^{15}NO instead of ^{14}NO) produced no detectable changes to the 2.016 or 2.027/1.976 signals (Figure 5), indicating that the contribution of NO to the main components of the spectra is small and indirect. In comparison, the effect of the isotopic replacement on the iminoxyl radical signal (presented here as a reference), produced by the interaction of NO with Y_D (*22*), is very pronounced (see inset of Figure 5).

A Light-Insensitive Signal Underlying the g = 2.016. A weak signal underlies the g = 2.016 one under certain conditions. The signal becomes obvious when a sample containing the g = 2.016 signal, Figure 6A, is transferred to +10 °C for 1 min (a procedure that results in the reversible loss of the g = 2.016 signal, as discussed in an earlier section), Figure 6b. The same signal can be obtained by prolonged (in the hours time scale) incubation at −30 °C in the dark without prior illumination, but generation of the g = 2.016 signal accelerates its formation. The new signal is insensitive to illumination or prolonged dark adaptation.

The new signal has a striking resemblance to EPR signals *o*f compounds with general formula $Fe(NO)_2(X)_2$ (X = a series of amino acids), as demonstrated by comparison in Figure 6C with the spectrum of $Fe(NO)_2$(imidazole)$_2$, synthesized according to ref *38*. Similar signals have been obtained in other non-heme iron proteins (see, e.g., refs *39*−

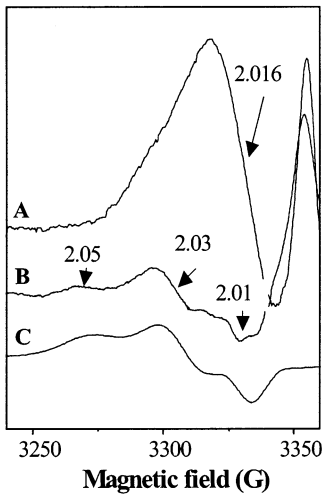

FIGURE 6: The residual, light-insensitive signal underlying the $g = 2.016$ one. (A) The $g = 2.016$ produced as in Figure 1; (B) the remaining signal following further incubation for 1 min at 10 °C; (C) the EPR spectrum of an $Fe(NO)_2(imidazole)_2$ complex. EPR conditions are the same as those in Figure 1.

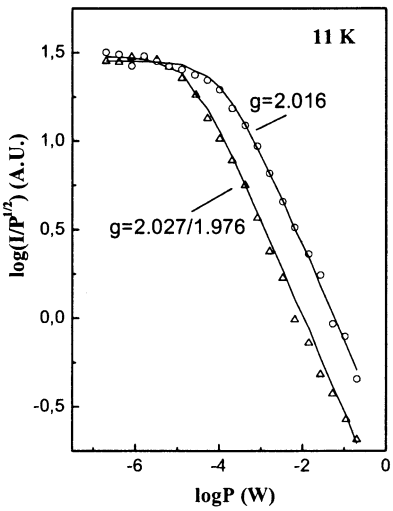

FIGURE 7: Microwave power dependence of the two main signals of the present study. Solid lines represent fittings with the formula given in the Materials and Methods.

41). The corresponding signal in mammalian ferritins classified as A type (practically identical *g*-values with the signal in Figure 6B) is attributed to iron−nitrosyl complexes with imidazole groups of histidine residues (*40*). A B-type signal in the same spectral region but with an axial **g**-tensor ($g_\perp = 2.033$, $g_{||} = 2.014$) has been attributed to iron−nitrosyl complexes with the thiol groups of cysteine residues (*40*). While an A-type signal is induced in PSII, a B-type signal was induced in control experiments with Photosystem I (preliminary experiments). Photosystem I is well-known to have a series of iron−sulfur electron acceptors.

The iron in the dinitrosyl complexes is usually described as Fe^{1+} ($3d^7$, $S = {}^1/_2$) or $Fe^{1-}(NO^+)_2$ (*42*). To form this complex in the present case, the iron is presumably reduced slowly by NO during prolonged storage at −30 °C and this is accompanied by the binding of two NO molecules. The much faster production of the complex in samples preilluminated at 200 K suggests that Q_A^- acts as a rapid reductant of the iron under these conditions.

Microwave Power Saturation of the Signals. A number of EPR signals are associated with the reduced quinone-iron complex, $Q_A^-Fe^{2+}$. These include the $g = 1.9$ and 1.82 signals (*12*, *13*), the formate-induced $g = 1.82$ signal (*15*) (oxalate also induces a similar signal (*34*)), and the cyanide induced signal at $g = 1.98$ (*9*). The signals of the $Q_A^-Fe^{2+}$(NO, F) complex (*11*) have been recently added to this list. When the iron is converted to spin zero by excess cyanide (*10*) or physically removed (*31*, *21*), the signal at $g = 2.0045$ from the free semiquinone, Q_A^-, is obtained. Apart from the difference in the *g*-values, which reflects changes in the coordination environment (and the spin state in the case of the NO) of the iron, these signals do not saturate easily, $P_{1/2} > 200$ mW. This is due to the strong magnetic coupling of the semiquinone with the iron. The single exception to this behavior is the free semiquinone signal, which saturates with a $P_{1/2}$ of 15 μW at 13 K (*10*).

The power dependence at 11 K of the two present signals is shown in Figure 7. The data are fitted as described in the Materials and Methods. At 11 K the $P_{1/2}$ of the 2.016 signal is 110 μW. This value is very low compared with the other $Q_A^-Fe^{2+}$ signals mentioned above but enhanced compared to the free semiquinone signal. In agreement with the enhanced $P_{1/2}$ value, the stimulated-echo decay is found to be fast, i.e., on the order of 3 μs at 5K. The decay rate usually expected for a free semiquinone radical in PSII at these temperatures is of the order of 8−11 μs. This reflects a relatively fast spin−lattice relaxation of the semiquinone electron spin. The $P_{1/2}$ of the (2.027, 1.976) signal is 10 μW, 1 order of magnitude less than that of the $g = 2.016$ signal. This $P_{1/2}$ value is actually comparable to that of the free semiquinone and indicates a negligible influence of the metal relaxer. The coupling with another spin in this case is indirectly inferred from the perturbation of the semiquinone signal.

Origin and Theoretical Simulations of the g = 2.016 and 2.027/1.976 EPR Signals. The above observations indicate that Q_A^- is directly involved in the $g = 2.016$ and 2.027/1.976 signals, while the influence of NO is indirect. The narrow width and the saturation of the signals at low power indicate a severely diminished influence of the iron spin—the iron in its unperturbed Fe^{2+} ($S = 2$) state exerts a strong influence both on the width and the saturation properties of the Q_A^- signals. This could result from a diminished magnetic coupling of the spin of the semiquinone with the spin of the iron and/or a decrease of the spin of the iron. Most likely, NO binds at the non-heme iron affording an iron nitrosyl complex. The competition studies indicate that this mode of binding must be different from the extensively studied slow binding of NO in the nonreduced state of the acceptor.

The iron−nitrosyl complex can have a spin of ${}^3/_2$ or a spin of ${}^1/_2$. The EPR properties of an Fe−NO ($S = {}^3/_2$) center interacting with an $S = {}^1/_2$ free radical have been discussed extensively (*11*). A very weak magnetic coupling of the two spins could produce broadened semiquinone spectra similar to the observed ones, but it should leave the Fe−NO ($S = {}^3/_2$) spectrum practically unmodified. Signals at $g = 4$ in variable amounts were present in some experiments, but these represented a small fraction of centers and were identical in shape to the signal, produced by the slow binding of NO to the non-heme iron in the nonreduced state of the quinone. The coupling model in (*11*) indicates that the $g = 2.016$

signal can be also reproduced assuming a stronger interaction, $J = 0.81$ cm^{-1} ($H_{ex} = J\mathbf{S_1}\cdot\mathbf{S_2}$), of Q_A^- with a $S = {}^3/_2$ system with $D > 5$ cm^{-1}, $E/D = 0$. Similarly, the $g = 2.027/1.97$ signal in the presence of CN^- can be reproduced within the same model with $E/D = 0.003$ and $J = 0.83$ cm^{-1}. An important shortcoming of this interpretation is, however, that the spin fraction contributing to the spectral region of the signals is very low, about 3−5%, while the integrated area of the experimental spectra represents about 50% of the PSII centers.

An alternative possibility is that the spin of the present iron−nitrosyl species is ${}^1/_2$. The spin Hamiltonian, which applies in this case, is

$$H = J\mathbf{S_1}\cdot\mathbf{S_2} + g_1\beta\mathbf{B}\cdot\mathbf{S_1} + \beta\mathbf{B}\cdot\mathbf{g_2}\cdot\mathbf{S_2}$$

where, $S_1 = {}^1/_2$ represents the spin of the semiquinone radical with $g_1 = 2.0045$ (isotropic), and $S_2 = {}^1/_2$ is the spin of the iron−nitrosyl complex, for which the **g** tensor, $\mathbf{g_2}$, is in general anisotropic. The exchange interaction, J, between the two spin species is approximately assumed isotropic.

First, we shall briefly summarize the salient EPR properties of the interaction of the two $S = {}^1/_2$ centers. For a recent more thorough and comprehensive analysis, the reader is referred to ref *43*. In the case of isotropic **g**-tensors, the critical parameter determining the EPR spectra of such a system is the ratio $\Delta g\beta B/J$, where Δg is the difference between the **g** tensors of the two $S = {}^1/_2$ centers. When this ratio is larger than or close to unity, one usually observes two strong central lines and two weaker ones at the wings, in an ABBA fashion. As this ratio is getting smaller, the two central lines become stronger and converge toward a single EPR line at $g = (g_1 + g_2)/2$, whereas the outer peaks become weaker and move toward lower and higher fields, respectively. In the case of one anisotropic tensor, $\mathbf{g_2}$, similar considerations can be made for each principal axis separately (*43*).

Simulation of the "g = 2.016" Signal. The observation of a single line for this signal Figure 1 suggests that the anisotropy of g_2 is relatively small (not resolved), and therefore the above discussion can be qualitatively applied if we replace $\mathbf{g_2}$ with the average value, $g_{2,ave}$, of this tensor. Accordingly, the presence of a single central peak and the absence of satellites indicates that the ratio $\Delta g\beta B/J$ is substantially small, and the zero crossing point at $g = 2.016$ is equal to $(g_1 + g_{2,ave})/2$. Assuming $g_1 = 2.0045$ for the semiquinone (*10*), we obtain accordingly $g_{2,ave} \sim 2.03$.

The restrictions set by the above considerations have been used as constraints in theoretical simulations of the signal. Figure 8A shows a simulation of the $g = 2.016$ signal with $g_1 = 2.0045$, $g_{2x} = 2.063$, $g_{2y} = 2.028$, $g_{2z} = 1.995$, $J = 0.025$ cm^{-1}, and $\sigma_B = 0.1$ mT. The reproduction of the line shape is clearly satisfactory, but this does not imply that this set of parameters is unique. It should be remembered that the critical parameter is the ratio $\Delta g\beta B/J$. Also, simulations of similar quality can be obtained (not shown) with an isotropic $\mathbf{g_2}$ tensor equal to 2.03, and assuming dipolar interactions between the two species with an inter-center distance of ∼10 Å. The unambiguous conclusion however is that the Fe−NO species is characterized by $g_{ave} \sim 2.03 > 2.00$. The calculated g_2 value rules also out the possibility that the second spin species is an NO moiety trapped at a site in the vicinity of Q_A^-. Such centers are characterized with $g < 2.00$ (*44*). Actually, if the site of binding of NO was different from the iron, one would have to explain the absence of an effect of the unperturbed iron on the Q_A^-−NO signal.

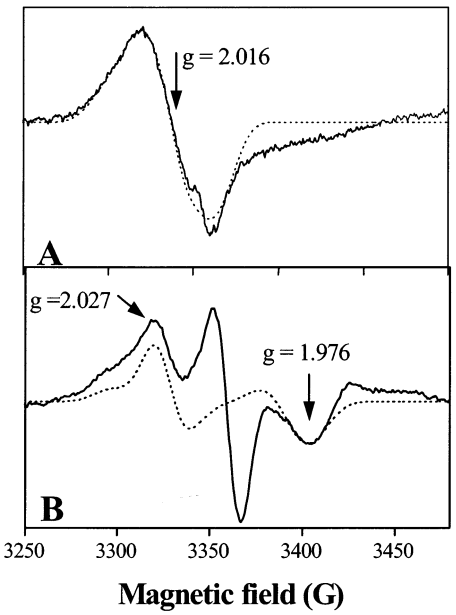

FIGURE 8: The $g = 2.016$ and 2.027/1.976 EPR signals (solid lines) and theoretical simulations (dotted lines). See text for details. The sloppy baseline in the high-field side of the experimental spectrum A is due to over-subtraction of the free-NO contribution (see Materials and Methods). The narrow contribution at $g = 2$ in the experimental spectrum B is due to a minority species. Experimental difference spectra obtained as in Figures 1 and 4.

Simulation of the g = 2.027/1.967 Signal. The $g = 2.027/1.976$ signal, Figures 4 and 8B, consists of a broad asymmetric absorption peak at $g = 2.027$ and a valley at $g = 1.98$. The details of the signal are not well resolved because of the presence of light-induced free radical signals at $g \sim 2.00$ and the broad free NO signal at $g < 2.00$. The presence of a peak at $g > 2.0$ and a valley at $g < 2.0$ can be interpreted in the context of a weak interaction between two $S = {}^1/_2$ species as above if we assume that the anisotropy of S_2 is not negligible. In this case the behavior of the spectrum is dictated by three ratios, $\Delta g_i\beta H/J$ (*43*), where $\Delta g_i = (g_{2i} - g_1)$, $i = x,y,z$, with $g_1 = 2.0045$. If these ratios are substantially small, then the resulting spectrum consists of an anisotropic spectrum with a peak at $g_x = (g_{2x} + g_1)/2$, a derivative at $g_y = (g_{2y}+g_1)/2$, and a valley at $g_z = (g_{2z}+g_1)/2$. We assign the $g = 2.027$ feature to the g_x peak of such as system, yielding $g_{2x} \sim 2.05$. Similarly, the $g = 1.98$ feature is assigned to the g_z-valley yielding $g_{2z} \sim 1.96$. For $g_{2y} \sim 2.00$ a derivative feature is expected at $g \sim 2.00$. The lack of such a feature in our spectra may be explained in a number of ways. Possible hyperfine interactions with a large component along the g_{2y} axis (see below) and/or dipolar interactions between the two $S = {}^1/_2$ centers would lead to a severe broadening of the $g = 2.00$ feature.

Figure 8B shows a simulation of the spectrum assuming $g_{2x} = 2.055$, $g_{2y} = 2.00$, $g_{2z} = 1.957$, $J = 0.05$ cm^{-1}, and a dipolar interaction with an intercenter distance of $r_{12} = 9.0$ Å, $\theta = 80^o$, $\phi = 90^o$, and a distribution in r_{12} of $\sigma_r = 0.5$ Å. θ and ϕ refer to the relative orientation of the vector $\mathbf{r_{12}}$ with respect to the principal axes of the tensor $\mathbf{g_2}$. The

Scheme 1: Molecular Model Illustrating the Different Modes of Binding of NO to the Iron Depending on the Oxidation State of the Primary Quinone, Q_A, and/or the Presence of Fluoride or Cyanide

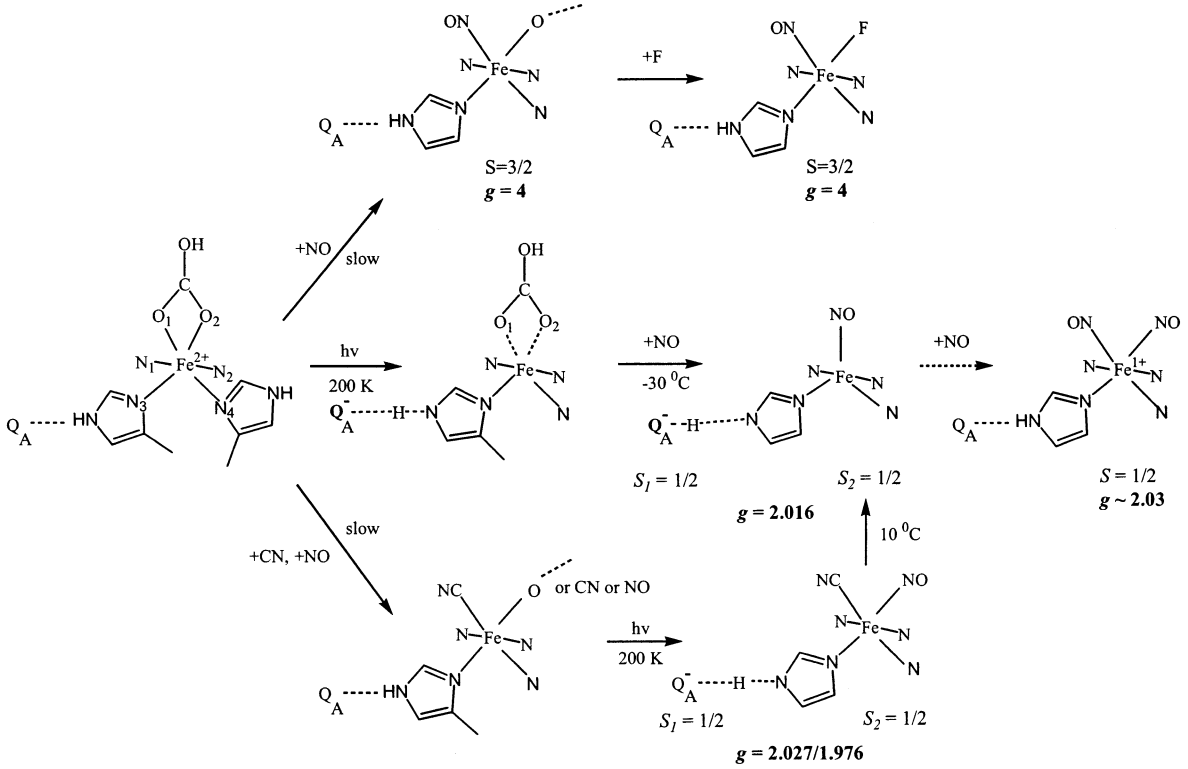

simulation reproduces the experimental spectrum quite satisfactorily, supporting the theoretical model adopted above. It is stressed, however, that the quoted parameters should be considered as indicative.

It is interesting that the derived *g*-values for the S_2 species are almost identical to those for the $E^r\cdot(CN)_{\geq 2}\cdot NO$ complex observed by Orville and Lipscomb in protocatechuate 3,4-dioxygenase (*45*). The *g* values of this complex are $g_x = 2.06$, $g_y = 2.00$, and $g_z = 1.96$. Hyperfine interactions from the N and C nuclei were also observed, and interestingly enough, A_y from the N nucleus of NO was found to be significantly larger than the other two components. Hyperfine interactions could not be resolved in our experimental spectra mainly due to uncertainties in the baseline at $g = 2.00$. Simulations of the $g = 2.027$ and 1.98 signal, including hyperfine interactions with values similar to those reported in (*45*), resulted in marginal improvements. Notably, the theoretical spectra were nondetectably affected at the $g = 2.027$ and 1.98 positions by the isotopic substitution ^{15}N for ^{14}N, as observed experimentally.

The exchange couplings deduced from the above analysis appear to be very small (approximately an order of magnitude smaller) compared with the couplings obtained in the case of the semiquinone coupling to the $S = {}^3/_2$ Fe−NO complex (*11*) or the case of the $Q_A^-Fe^{2+}$ complex in the purple bacteria (*16*, *17*). It has been proposed that a mechanism for altering the exchange between the Q_A^- and the non-heme iron is the modification of the H-bond strength between the Q_A^- and the His215 residue (one of the four that ligate the non-heme iron in PSII) (*32*): strengthening of the H-bond to the imidazole−iron results in a more strongly coupled system, and vice-versa. This idea is corroborated by EPR data in *R. sphaeroides*, where the non-heme iron has been replaced by Cu^{2+} (*46*) and is consistently supported by the considerations that follow in the molecular model.

A Molecular Model. Scheme 1 summarizes the reactions of NO with the non-heme iron in the context of a molecular model. Bicarbonate is assumed to bind as a bidentate ligand in the untreated Fe^{2+} state, assuming analogy with the bidentate glutamate residue in the purple bacteria (*41*) and on the basis of FTIR studies in PSII (*6*). Starting from the untreated state of the complex, three possible routes are shown depending on the redox state of Q_A and the presence or absence of cyanide.

Upper Route. Incubation with NO in the Q_AFe^{2+} state of the complex results in the slow displacement of bicarbonate by NO and formation of the well-characterized $g = 4$ iron−nitrosyl species, indicative of an $S = {}^3/_2$ spin state (*7*). The iron−nitrosyl complex is assumed to be six-coordinate with an oxygen ligand derived, e.g., from water or bicarbonate. Fluoride can replace the sixth ligand, giving rise to an $S = {}^3/_2$ complex with somewhat greater rombicity and pronounced hyperfine splitting from the fluoride nucleus (*11*).

Middle Route. An important aspect of the chemistry leading to the evolution of the $g = 2.016$ signal is that formation of Q_A^- weakens the iron bicarbonate bond and allows for the competitive binding of NO. This assumption is supported by the observations discussed in the section describing the effects of carboxylate anions on the 2.016 signal and is justified by the following considerations. Reduction of Q_A to the semiquinone by illumination is expected to cause a shift of the hydrogen-bonding proton (*47*) from imidazole (His215 of the D1 protein) toward the semiquinone radical. This in turn lowers the positive charge on the iron and causes a weakening of the Fe−bicarbonate bond (trans influence). NO, which is an electrophile, can

efficiently displace this ligand. The new $\{Fe-NO\}^7$ complex is characterized by an $S = {}^1/_2$ ground state, which by interaction with the semiquinone radical gives rise to the characteristic EPR signal at $g = 2.016$. The above considerations show analogy (reverse) to the regulation of the pK_a of D1His215 (the histidine closest to Q_B) by bicarbonate, inferred from FTIR studies (*48*).

Numerous $\{FeNO\}^7$ synthetic complexes with ground states of $S = {}^1/_2$ can be found in the literature (*49*−*53*). Most of these complexes are, however, characterized by strong ligands, that favor low-spin states of the iron even in the absence of NO. The present configuration (an Fe−NO transient in proximity to a semiquinone radical trapped at −30 °C) appears to have no direct analogue in the literature. Of special interest are two compounds studied recently (*52*, *53*). In the tropocoronand complex Fe(NO)(TC-5,5) (*52*), the iron atom is five-coordinate in a trigonal bipyramidal geometry with the NO in the equatorial plane. The Fe−N−O bond angle is almost linear (174°). This complex is best described as an $Fe^{3+}(S = {}^1/_2)-NO^-(S = 1)$ antiferromagnetically coupled pair yielding an $S = {}^1/_2$ ground state. In the *trans*-[(cyclam)Fe(NO)(Cl)](ClO_4) complex (*53*), the iron atom is six-coordinate, and the Fe−N−O angle bond is bent (144°). The iron−nitrosyl complex is described in this case as an $Fe^{3+}(S = {}^3/_2) - NO^-(S = 1)$ antiferromagnetically coupled pair. It is not clear which of these two synthetic complexes is more relevant to our case, but the geometry of the Fe(NO)(TC-5,5) complex (*52*) offers an attractive possibility consistent with a number of observations. It is reasonably assumed that the geometry of the untreated Fe^{2+} ligand environment in PSII is not too different from the bacteria. Extrapolating to Scheme 1, the Fe−N_3, Fe−N_4, Fe−O_1, and Fe−O_2 bonds all lie on the same plane, while the N_1−Fe−N_2 direction is approximately perpendicular to the plane. Furthermore, the line that bisects the two Fe−O bonds makes approximately a 120° angle with each of the Fe−N_3 and Fe−N_4 bonds. If NO binding displaces bicarbonate completely, then the iron would naturally assume a trigonal-bipyramidal geometry with the NO ligand occupying an equatorial position. This is the same arrangement with the Fe(NO)(TC-5,5) complex (*52*), and it is possible that the present complex is also described as $Fe^{3+}(S = {}^1/_2)-NO^-(S = 1)$. This configuration would favor a further shift of the hydrogen bonding proton to Q_A^- resulting probably in a weaker H-bond.

Further chemistry beyond the $g = 2.016$ configuration appears to occur with lower probability. A second NO molecule binds and the iron is presumably reduced by the semiquinone, yielding a dinitrosyl complex responsible for the signal with a g value of approximately 2.03, described in the experiment of Figure 6. This dinitrosyl complex can also form more slowly in the absence of the semiquinone Q_A^-. In this case excess NO could act as the reductant of the iron complex.

It might be argued that the Fe−NO complex in the $g = 2.016$ configuration is also a dinitrosyl complex magnetically interacting with the semiquinone. A third NO molecule would have to act as the reductant of the iron in this case. Although this possibility cannot be totally excluded, one would expect that prolonged preincubation with NO, to allow for the full evolution of the mononitrosyl $g = 4$ ($S = {}^3/_2$, upper route) complex, would speed up formation of the $g = 2.016$ species. The $g = 4$ configuration (and to a lesser extent the $g = 4$ in the presence of fluoride) appears indeed to convert to the $g = 2.016$ one following illumination and incubation at − 30 °C, but the size or speed of formation of the $g = 2.016$ signal is independent of the size of the precursor $g = 4$ signal (provided that the ambient concentration of NO is not limiting). The present phenomenology favors accordingly a mononitrosyl−iron complex, but this assignment may be considered tentative.

Lower Route. Modest concentrations of cyanide (see discussion related to the experiment of Figure 4) inhibit induction of the $g = 4$ signal ($S = {}^3/_2$) by NO (*9*, *10*). We suggest in Scheme 1 that under these conditions cyanide binds to the iron displacing one of the oxygen ligands. The identity of the sixth ligand is not clear, but depending on the relative concentrations, it could be monodentate bicarbonate or a second cyanide molecule or NO in a small fraction of centers. Formation of Q_A^- by subsequent illumination at 200 K favors displacement of the sixth anionic ligand by NO and formation of the species that produces the $g = 2.027/1.976$ signals. In cases of short preincubation with CN^- and NO, equilibrium binding has not been achieved and additional incubation at − 30 °C is required in order to obtain the maximum signal. The simultaneous binding of CN^- and NO would favor a low spin state of the iron. The similarity of this complex with the $E^r{\cdot}(CN)_{\geq 2}{\cdot}NO$ complex studied by Orville and Lipscomb in protocatechuate 3,4-dioxygenase (*36*) was noted already during the theoretical simulation of the spectra. The electronic distribution in this complex is not obvious. The fact that the spectrum of the Q_A^-−Fe−CN−NO complex (signal at $g = 2.027/1.976$) saturates at very low microwave powers, 10 μW compared with 110 μW for the Fe−NO complex yielding the $g = 2.016$ signal, would favor an $Fe^{2+}(S = 0)-CN^-NO(S = {}^1/_2)$ configuration.

It is interesting that warming up to 10 °C and subsequent incubation at −30 °C (within the lifetime of Q_A^-) results in the conversion of the $g = 2.027/1.976$ to the $g = 2.016$ configuration, the latter being presumably a more relaxed configuration. Since bicarbonate is displaced in the $g = 2.027/1.976$ configuration, this observation adds extra support to the assumption of the complete displacement of bicarbonate in the $g = 2.016$ configuration, too.

In conclusion, the present results reveal new modes of NO binding to the non-heme iron of PSII, which are favored in the reduced state of the quinone−iron complex. The results imply that reduction of Q_A has a trans influence on the postulated iron−bicarbonate bond inducing a significant weakening of it. This finding could have implications in understanding the mechanism of electron transfer in the acceptor side of PSII and the suggested physiological control exerted by bicarbonate.

ACKNOWLEDGMENT

The EPR simulation software was kindly provided by M. Hendrich (Carnegie Mellon University).

SUPPORTING INFORMATION AVAILABLE

Three figures, S1−S3, describing experiments not shown in the main manuscript. This material is available free of charge via the Internet at http://pubs.acs.org.

REFERENCES

1. Diner, B. A., and Babcock, G. T. (1996) in *Advances in Photosynthesis: Oxygenic Photosynthesis: The Light Reactions* (Ort, D. R., and Yocum, C. F., Eds.) Vol. 4, pp 213−247, Kluwer Academic Publishers, Dordrecht, The Netherlands.
2. Diner, B. A., Petrouleas, V., and Wendoloski, J. J. (1991) *Physiol. Plant. 81*, 423−436.
3. Zouni, A., Witt, H. T., Kern, J., Fromme, P., Krauss, N., Saenger, W., and Orth, P. (2000) *Nature 409*, 739.
4. Deisenhofer, J., and Michel, H. (1989) *EMBO J. 8*, 2149−2169.
5. Petrouleas, V., and Diner, B. A. (1990) *Biochim. Biophys. Acta 1015*, 131−140.
6. Hienerwadel, R., and Berthomieu, C. (1995) *Biochemistry 34*, 16288−16297.
7. Diner, B. A., and Petrouleas, V. (1990) *Biochim. Biophys. Acta 1015*, 141−149.
8. Petrouleas, V., Sanakis, Y., Deligiannakis, Y., and Diner, B. A. (1992) in *Research in Photosynthesis* (Murata, N., Ed.) Vol. II, p 119, Kluwer, Dordrecht, The Netehrlands.
9. Koulougliotis, D., Kostopoulos, T., Petrouleas, V., and Diner, B. A. (1993) *Biochim. Biophys. Acta 1141*, 275−282.
10. Sanakis, Y., Petrouleas, V., and Diner, B. A. (1994) *Biochemistry 33*, 9922−9928.
11. Sanakis Y., Petasis, D., Petrouleas, V., and Hendrich, M. (1999) *J. Am. Chem. Soc. 121*, 9155−9164.
12. Nugent, J. H. A., Diner, B. A., and Evans, M. C. W. (1981) *FEBS Lett. 124*, 241.
13. Rutherford, A. W., and Zimmerman, J. L. (1984) *Biochim. Biophys. Acta 767*, 168.
14. Nugent, J. H. A., Doetschman, D. C., MacLachlan, D. J. (1992) *Biochemistry 31*, 2935−2941.
15. Vermaas, W. F. J., and Rutherford, A. W (1984) *FEBS Lett. 175*, 234.
16. Butler, W. F., Calvo, R., Fredkin, D. R., Isaacson, R. A., Okamura, M. Y., and Feher, G. (1984) *Biophys. J. 45*, 947−973.
17. Dismukes, G. C.; Frank, H. A.; Friesner, R.; Sauer, K. (1984) *Biochim. Biophys. Acta 764*, 253−271.
18. Berthold, D. A., Babcock, G. T., and Yocum, C. F. (1981) *FEBS Lett. 134*, 231.
19. Ford, R. C., and Evans, M. C. W. (1983) *FEBS Lett. 160*, 159.
20. Fauth, J. M., Schweiger, A., Braunschweiler, L., Forrer, J., and Ernst, R. (1986) *J. Magn. Reson. 66*, 64.
21. Deligiannakis, Y., Jegerschöld, C., and Rutherford, A. W. (1997) *Chem. Phys. Lett. 270*, 564.
22. Sanakis, Y., Goussias, Ch., Mason, R., and Petrouleas, V. (1997) *Biochemistry 36*, 1411−1417.
23. Demeter, S., Goussias, Ch., Bernat, G., Kovacs, L., and Petrouleas, V. (1993) *FEBS Lett. 336*, 352−356.
24. Goussias, Ch., Ioannidis, N., and Petrouleas, V. (1997) *Biochemistry 36*, 9261−9266.
25. Gilchrist, M. L., Bail, J. A., Randall, D. W., and Britt, R. D. (1995) *Proc. Natl. Acad. Sci. U.S.A. 92*, 9545.
26. Dikanov, S. A., and Tsvetkov, Y. D. (1992) *ESEEM Spectroscopy*, CRC Press, Boca Raton, FL.
27. Flanagan, H. L., and Singel, D. J. (1987) *J. Chem. Phys. 87*, 5606.
28. Dikanov, S. A., Tsvetkov, Y. D. Bowman, M. K., and Astashkin, A. V. (1992) *Chem. Phys. Lett. 90*, 149.
29. Mims, W. B., and Peisach, J. (1981) *Biological Magnetic Resonance*, Vol. 3, Chapter 5, Plenum Press, New York.
30. Astashkin, A. V., Hara, H., Kuroiwa, S., Kawamori, A., and Akabori, K. (1998) *J. Chem. Phys. 108*, 10143.
31. Peloquin, J. M., Tang, X.-S., Diner, B. A., and Britt, R. D. (1999) *Biochemistry 38*, 2057.
32. Deligiannakis, Y., Hanley, J., and Rutherford, A. W. (1999) *J. Am. Chem. Soc. 121*, 7563.
33. Edmonds, D. T. (1977) *Phys. Rep. C 29*, 233.
34. Deligiannakis, Y., Petrouleas, V., and Diner, B. A. (1994) *Biochim. Biophys. Acta 1188*, 260−270.
35. Petrouleas, V., Deligiannakis, Y., and Diner, B. A.(1994) *Biochim. Biophys. Acta 1188*, 271−277.
36. Zimmerman, J. L., and Rutherford (1986) *Biochim. Biophys. Acta 851*, 416−423.
37. Petrouleas, V., and Diner, B. A. (1987) *Biochim. Biophys. Acta 893*, 126−137.
38. Woolum, J. C., Tiezzi, E., and Commoner, B. (1968), *Biochim. Biophys. Acta 160*, 311.
39. Drapier, J.-C., Pellat, C., and Henry, Y. (1991) *J. Biol. Chem. 266*, 10162−10167.
40. Lee, M., Arosio, P., Cozzi, A., and Chasteen, N. D. (1994) *Biochemistry 33*, 3679−3687.
41. LeBrun, N. E., Andrews, S. C., Moore, G. R., and Thomson, A. J. (1997) *Biochem. J. 326*, 173−179.
42. Bryar, T. R., and Eaton, D. R. (1992) *Can. J. Chem. 70*, 1917−1926.
43. Fournel, A., Gambarelli, S., More, C., Asso, M., Chouteau, G., Hille, R., and Bertrand, P. (1998) *J. Chem. Phys. 109*, 10905.
44. Kasai, P. H., and Bishop, R. J., Jr. (1972), *J. Am. Chem. Soc. 94*, 5560.
45. Orville, A. M., and Lipscomb, J. D. (1997) *Biochemistry 36*, 14044−14055.
46. Calvo, R., Passegi, M. C. G., Isaacson, R. A. Okamura, M. Y., and Feher, G. (1995) *Biophys. J. 58*, 149.
47. Noguchi, T., Inoue, Y., and Tang, X. S. (1999) *Biochemistry 39*, 399−403.
48. Berthomieu, C., and Hienerwadel, R. (2001) *Biochemistry 40*, 4044−4052.
49. Hodges, K. D., Wollmann, R. G., Kessel, S. L., Hendrickson, D. N., Van Derveer, D. G., and Barefield, E. K. (1979) *J. Am. Chem. Soc. 101*, 906−917.
50. Fitzsimmons, B. W., Larkworthy, L. F., and Rogers, K. A. (1980) *Inorg. Chim. Acta 44*, L53-L54.
51. Wells, F. V., McCann, S. W., Wickmann, H. H., Kessel, S. L., Hendrickson, D. N., and Feltham, R. D. (1982) *Inorg. Chem. 21*, 2306−2311.
52. Franz, K. J., and Lippard, S. J. (1999) *J. Am. Chem. Soc. 121*, 10504−10512.
53. Hauser, C., Glaser, T., Bill, E., Weyhermuller, T., and Wieghardt, K. (2000) *J. Am. Chem. Soc. 122*, 4352−4365.

BI026223E